Journal of Wind Engineering & Industrial Aerodynamics xxx (xxxx) xxx

Contents lists available at ScienceDirect

Journal of Wind Engineering & Industrial Aerodynamics

journal homepage: www.elsevier.com/locate/jweia

Background/Resonant decomposition of the stochastic torsional flutter response of an aeroelastic oscillator under buffeting loads

Julien Heremans, Anass Mayou, Vincent Denoël *

Structural and Stochastic Dynamics, Structural Engineering, University of Liège, Belgium

ARTICLE INFO

Keywords:
Multiple timescale spectral analysis
Flutter
Galloping
Divergence
Aeroelastic instability

ABSTRACT

The complete flutter analysis of a structure requires the repeated analysis of the aeroelastic response of the structure for various wind velocities. In a spectral approach, each of these analyses is based on the integration of the power spectral density of the aeroelastic response. Traditional integration methods struggle to efficiently estimate these integrals because of the marked peakedness of the function in the neighborhood of the poles of the system. In this paper, we have derived an extension of the Background/Resonant decomposition (which is commonly applied under the quasi-steady assumption), to aeroelastic analysis, where the stiffness and damping of the coupled system changes with frequency. Both the background and resonant components take a more general form than in the well known case. They remain simple, however, and offer therefore a straightforward understanding of the response. The proposed formulation is illustrated with several examples of torsional flutter, where the critical state corresponds either to torsional galloping either to divergence. The study is limited to single degree-of-freedom systems but constitute the cornerstone of an extension to multi degree-of-freedom systems, where such an approximation becomes very interesting in terms of computational efficiency.

1. Introduction

Last few decades have seen large progress in long span bridge engineering, inviting civil engineers to design constantly more slender structures, with innovative shapes. Among all the tasks in the design of such long span bridges, flutter is recognized as a concerning issue.

The first modeling of bridge flutter was inspired by the works on the flat plate (Theodorsen, 1935) to study the behavior of airfoils in aeronautics. Few decades later, research migrated to civil engineering (Scanlan and Tomo, 1971) and reached a canonical formulation (Scanlan, 1993), applicable to the complex profiles encountered in bridge engineering (Sarkar et al., 1992, 2009). Scanlan's notation relates to the self-excited forces, where the lift force, the drag force and the pitching moment are expressed by means of the so-called *flutter derivatives*, which are obtained experimentally in a wind tunnel or by means of numerical simulations. These quantities can be used to compute the aeroelastic response of large bridges, which covers both the determination of the critical wind velocity (e.g. (Miyata and Yamada, 1990)) and the response to buffeting including the unsteady aerodynamics. At a final stage of a bridge design, it is indeed important to have a detailed computation of the bridge response, including structural modes shapes, computed with the finite element method or simple analytical expressions, as well as their evolution with the mean wind velocity (Jain et al., 1996; Katsuchi et al., 1998; Chen et al., 2000; Chen and Kareem, 2008). At the opposite, simple models are also necessary to assess and understand the dynamical behavior of structures under wind loading. The Background/Resonant (B/R) decomposition for the quasi-steady response to gusty winds (Davenport, 1962) is an example of a simple but commonly used approach to assess and understand the response of structures to buffeting. The simplicity of such models is appreciated especially in the preliminary design stage or in a probabilistic context where these operations have to be repeated a large amount of times (Cheng et al., 2005; Tommaso et al., 2014). As to flutter, the most popular of these simple models is the pitch-plunge model (Bisplinghoff and Ashley, 2013; Dimitriadis, 2017; Amandolese et al., 2013), where the structure is reduced to a two degree-of-freedom system and is subjected to both a lift force and a pitching moment, whereas the drag force is not considered. This model is easier to understand (Chen, 2007) but can be further simplified to a single degree-of-freedom model, in cases where the response takes place in only one mode. This later situation is the simplest case where divergence and galloping can be observed (Simiu and Scanlan, 1996; Hémon, 2006).

* Corresponding author.
E-mail address: v.denoel@uliege.be (V. Denoël).

https://doi.org/10.1016/j.jweia.2020.104423
Received 16 July 2020; Received in revised form 12 October 2020; Accepted 12 October 2020
Available online xxxx

This review of the literature, and similar more involved state-of-the-art reviews (Abbas et al., 2017; Diana et al., 2019), depicts the available methods for the flutter analysis of a bridge deck subjected to aerodynamic and buffeting loads. The aeroelastic analysis is conducted either in the time domain through the simulation of wind realizations, either in the frequency domain in the form of a spectral analysis. In both cases, the design quantity of interest is the variance of the response in several modes or at several locations along the deck. In the time domain analysis, the variance is simply obtained by a statistical processing of time series. In the spectral analysis, the variance is the result of the integration of the corresponding power spectral density. In the literature, this operation is achieved by means of standard integration procedures where a fine frequency resolution must be set to properly capture the sharp resonance peaks. This operation is similar to the determination of the variance of the response under buffeting loading only, which is known to benefit from the (B/R) decomposition (Davenport, 1962). In its current and original formulation, this decomposition is only valid, though, for structures with fixed natural frequency and damping ratio. This paper explores the possibility to extend this well-established decomposition to the spectral analysis of a simple aeroelastic system. The proposed approach is based on the general theory of the Multiple Timescale Spectral Analysis (Denoël, 2015), which generalizes the concept to much broader domains of application (e.g. (Denoël and Degée, 2009; Denoël, 2009; Denoël, 2011)).

In this paper, we will limit the analysis to the response of a single degree-of-freedom system in the frequency domain. This is the first step toward the construction of a complete, rapid and insightful analysis of large structural models which could be studied in a modal basis. On top of the proposed solution derived in this paper, an extension of the modal coupling (Denoël, 2009) would be necessary. This aspect is unfortunately not covered in this paper. It is organized as follows. Section 2 presents the mathematical problem that is solved with the Multiple Timescale Spectral Analysis. Section 3 derives the ad hoc solution while some illustrative examples are given in Section 4.

2. Problem statement

2.1. Governing equations

The dynamics of a single degree-of-freedom system subjected to buffeting and aerodynamic loads is governed by

$$m_s\ddot{q}(t) + c_s\dot{q}(t) + k_s q(t) = f_{bu}(t) + f_{ae}(t), \tag{1}$$

where m_s, c_s and k_s are the mass, viscosity and stiffness of the structural system, and where t is the time. The loading consists of a buffeting loading $f_{bu}(t)$ which is here assumed to be characterized as a Gaussian stochastic process (Simiu and Scanlan, 1996) and the aerodynamic loading $f_{ae}(t)$, which takes the form

$$f_{ae}(t) = \mathcal{L}_{c_{ae}}[\dot{q}(t)] + \mathcal{L}_{k_{ae}}[q(t)], \tag{2}$$

where $\mathcal{L}_{c_{ae}}[\cdot]$ and $\mathcal{L}_{k_{ae}}[\cdot]$ represent linear time invariant operators. They are usually expressed in the time domain by means of indicial functions (Sarkar et al., 1992; Tubino, 2005). By gathering them on the lefthand side, the governing equation reads

$$m_s\ddot{q}(t) + c_s\dot{q}(t) - \mathcal{L}_{c_{ae}}[\dot{q}(t)] + k_s q(t) - \mathcal{L}_{k_{ae}}[q(t)] = f_{bu}(t) \tag{3}$$

The frequency domain formulation is equivalent since operators $\mathcal{L}_{c_{ae}}[\cdot]$ and $\mathcal{L}_{k_{ae}}[\cdot]$ are linear. In the frequency domain, the governing equation becomes

$$\left[-m_s\omega^2 + \mathrm{i}\omega\, c(\omega) + k(\omega)\right] Q(\omega) = F_{bu}(\omega), \tag{4}$$

where $c(\omega) = c_s - c_{ae}(\omega)$ and $k(\omega) = k_s - k_{ae}(\omega)$ gather both the structural and aerodynamic viscosity and stiffness. It is obtained by a side-by-side Fourier transform of (3). It is readily seen that $c_{ae}(\omega)$ and $k_{ae}(\omega)$ correspond to the frequency response functions associated with the linear operators $\mathcal{L}_{c_{ae}}[\cdot]$ and $\mathcal{L}_{k_{ae}}[\cdot]$. They depend on the frequency as a consequence of the unsteadiness of the aerodynamic forces (Kareem and Tamura, 2013). Some specific cases such as the flat plate model developed in the works of Theodorsen (1935) are discussed in Section 4.2. Other examples will include the Scanlan's coefficients.These coefficients are supposed to be known, typically from wind tunnel measurement or computational fluid dynamics simulations. This Section is meant to be more general; so symbols $c_{ae}(\omega)$ and $k_{ae}(\omega)$ are kept throughout the derivation.

The mean wind loading is treated separately in a static analysis. The buffeting loading $f_{bu}(t)$ is therefore considered to be zero-mean. Since it is assumed to be a Gaussian process, it is completely characterized by its power spectral density $S_{f,bu}(\omega)$. The power spectral density of the response $q(t)$ is thus obtained by

$$S_q(\omega) = |H(\omega)|^2 S_{f,bu}(\omega), \tag{5}$$

where

$$H(\omega) = \left[-m_s\omega^2 + \mathrm{i}\omega\, c(\omega) + k(\omega)\right]^{-1} \tag{6}$$

is the frequency response function of the aeroelastic system. The variance of the response is finally obtained by integration of (5)

$$\sigma_q^2 = \int_{-\infty}^{+\infty} S_q(\omega)\mathrm{d}\omega. \tag{7}$$

2.2. Structural analysis under buffeting and flutter

In many wind engineering applications (as seen in the illustrations presented in Section 4), $c_{ae}(\omega)$ and $k_{ae}(\omega)$ are expressed as a function of the reduced frequency $K = \omega B/U$ where B is a characteristic size of the structural element (a bridge deck) and U is the average wind velocity. In this paper, it is implicitly assumed that both $c_{ae}(\omega; U, B)$ and $k_{ae}(\omega; U, B)$ are functions of the wind velocity too, although this is not explicitly written in order to lighten the notations.

As a consequence, the variance of the response (7) can be computed for several values of the wind velocity. However, the analysis of a structure under buffeting loads and in the framework of the quasi-steady assumption is usually performed for the design wind speed only (EN, 2009) and very little care is given to smaller values of the wind velocity since, in that case, the standard deviation of the response σ_q is proportional to the wind velocity (for constant turbulence intensity) (Simiu and Scanlan, 1996), see Fig. 1-a; so the worst case is certainly captured when the wind speed is the design wind speed.

The unsteady formulation of the aerodynamic forces, see (2), might lead to aeroelastic instabilities such as galloping or divergence, both of which are covered by the more general terminology of flutter (Hémon, 2006; Bisplinghoff and Ashley, 2013). Galloping occurs when the wind velocity is such that the aerodynamic damping cancels the structural damping, so that the total damping $\bar{\xi}$ is null at the natural circular frequency $\bar{\omega}$ of the aeroelastic system. The corresponding critical wind velocity $U_{gal.}$ is obtained by solving

$$c(\bar{\omega}) = c_s - c_{ae}\left(\bar{\omega}\left(U_{gal.}\right)\right) = 0, \tag{8}$$

where $\bar{\omega}\left(U_{gal.}\right)$ is the natural frequency of the aeroelastic system, see details next. Divergence occurs when the aerodynamic stiffness cancels the structural stiffness, so that the total stiffness, henceforth the natural frequency of the aeroelastic system, vanishes. The corresponding critical wind velocity is obtained by solving

$$k(\bar{\omega}) = k_s - k_{ae}\left(\bar{\omega}\left(U_{div.}\right)\right) = 0, \tag{9}$$

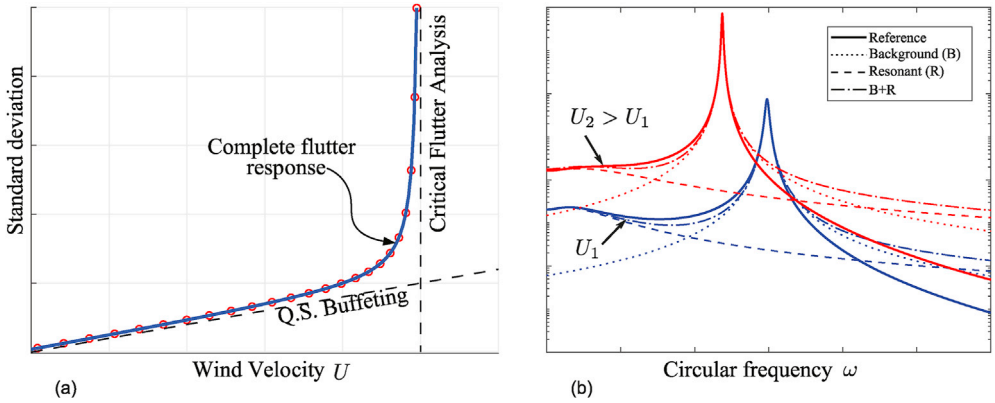

Fig. 1. Illustration of background/resonant (B/R) method applied to flutter analysis. (a) Effect of wind speed on the displacement standard deviation and associated limit cases (b) Background/resonant decomposition of a displacement PSD.

where $\overline{\omega}(U_{\text{div.}}) = 0$ is the natural frequency of the aeroelastic system corresponding to wind velocity $U_{\text{div.}}$.

The integral defined in (7) does not converge in the sense of Riemann for $U = U_{\text{gal.}}$ since there is a non-integrable singularity located at $\omega = \overline{\omega}(U_{\text{gal.}})$ and it does not converge either for $U = U_{\text{div.}}$ since there is a non-integrable singularity located at $\omega = 0$. A usual flutter analysis consists in solving an eigen value problem to determine the critical wind velocities. The smallest of the critical wind velocities gives the flutter onset instability.

Beside the response to quasi-steady buffeting and the determination of the critical wind velocity as an eigen value problem, which are represented in Fig. 1-a with dashed lines, a third type of analysis includes both the buffeting and unsteady wind forces at the same time, see (1). In that case, the transition from the quasi-steady to the unsteady response is determined (Scanlan and Jones, 1990). To reproduce the complete flutter response requires to repeat the computation of the integral (7) for various values of the wind velocity. The added value of the complete flutter response is that it provides the magnitude of the structural response for wind velocities that go beyond the domain of validity of the quasi-steady domain, and which correspond to about 50%–80% of the flutter speed. Indeed, in typical design codes it is required that the critical flutter velocity is at least 1.25 times larger that the design wind speed, e.g. (EN, 2009). The knowledge of the response in this intermediate regime allows to classify the flutter into soft or hard flutter categories (Zhang, 2007). This is an important information for the designers.

In summary, the determination of the complete flutter response of a structure, as considered in this paper, is a mathematical problem that consists in solving a dynamical system with frequency-dependent stiffness and viscosity for a repeated number of wind velocities in the range $[0, U_{\text{cr}}]$.

2.3. Motivation and proposed approach

The numerical evaluation of (7), complicated by the presence of two sharp resonance peaks, must be performed with a high frequency resolution. Also the integration range cannot be pushed to infinity but must be sufficiently large to properly capture both the background and resonant components. Therefore, the calculation of the variance (7) using conventional integration techniques (Press et al., 2007) requires many integration points and becomes particularly unsuitable for complex models where the computational cost of every integration point is significant. Furthermore, the derivation of alternative and lighter methods for the evaluation of (7) becomes of primary interest as soon as the variance must be computed a large number of times, such as in a complete flutter analysis.

In this paper, we seek to develop a multiple timescale approximation (Hinch, 1991) of the integral, in the manner of the (B/R) decomposition (Davenport, 1962). The main difference is that the viscosity and stiffness of the aeroelastic system vary with the frequency, while they are supposed to be constant in the original formulation. The principle relies on the semi-analytical integration of two components, background and resonant, which are identified as the two main contributions to the integral. Fig. 1-b illustrates the decomposition for two different wind velocities. As the wind velocity increases, the natural frequency might shift off, the damping ratio might also drop; these are the new features that are captured by the formulation proposed in the following Section and that are absent from the original (B/R) decomposition. It is also desired to accommodate the possible variation of the aerodynamic viscosity and stiffness across the resonance peak, since $c(\omega)$ and $k(\omega)$ are functions of the frequency in the aeroelastic problem. This is an important specificity of the considered problem, which differs from the original (B/R) decomposition, where $c(\omega)$ and $k(\omega)$ were assumed to be constant.

3. Multiple Timescale Spectral Analysis

3.1. Assumptions

The approximate solution is based on the following assumptions:

(i) the timescales of the loading and of the system are significantly different. In other words, a distinction is made between the slow dynamics represented by the buffeting loading, and fast dynamics represented by the natural vibrations of the aeroelastic system. The centroid of the power spectral density of the buffeting load shall be substantially lower (5–10 times lower) than the natural frequency of the aeroelastic system;

(ii) the structural damping ratio is small, smaller or of the same order of magnitude as 5%–10%; the quality of the approximation worsens as the damping ratio grows beyond these values;

(iii) the frequency dependent stiffness and damping $k(\omega)$ and $c(\omega)$ vary smoothly and moderately in the neighborhood of the resonance peak of the aeroelastic system. The exact meaning of this assumption will be made clearer after introduction of the dimensionless formulation.

Assumptions (i) and (ii) are the same as in the classical (B/R) decomposition, while assumption (iii) is specific to the current problem. Under these conditions, the general framework of the Multiple Timescale Spectral Analysis can be specialized to get simple solutions. In order to make these assumptions explicit, we define the dimensionless aeroelastic stiffness and viscosity as

$$\mathcal{K}(\omega) := \frac{k(\omega)}{k_{\text{s}}} = 1 - \frac{k_{\text{ae}}(\omega)}{k_{\text{s}}} \quad \mathcal{C}(\omega) := \frac{c(\omega)}{c_{\text{s}}} = 1 - \frac{c_{\text{ae}}(\omega)}{c_{\text{s}}} \tag{10}$$

which are frequency dependent and are not necessarily small; in fact the aerodynamic loading can significantly affect the natural frequencies. We also assume that the structural damping ratio ξ_s is a small positive number,

$$\xi_s := \frac{c_s}{2\sqrt{k_s m_s}} \ll 1. \tag{11}$$

This is the small parameter of the problem that will be used in the subsequent analysis. It is here explicitly introduced in order to formalize Assumption (i). With these notations, the frequency response function of the aeroelastic system becomes

$$H(\omega) = \frac{1}{k_s}\left(-\frac{\omega^2}{\omega_s^2} + 2\mathrm{i}\xi_s\frac{\omega}{\omega_s}\mathcal{C}(\omega) + \mathcal{K}(\omega)\right)^{-1}, \tag{12}$$

where $\omega_s := \sqrt{k_s/m_s}$ is the natural circular frequency of the structure in wind-off conditions.

3.2. The background component

The Background component corresponds to the contribution of the variance which is located in the very low frequency range, in the neighborhood of the centroid of the power spectral density of the buffeting load, see Fig. 1-b. In this area, $\omega \ll \omega_s$, the frequency response function of the aeroelastic system is locally approximated by $\hat{H}(\omega) = (k_s\mathcal{K}(\omega))^{-1}$, which is obtained by neglecting the dynamics in the system (*i.e.* quasi-static response). The first contribution to the power spectral density of the response is therefore given by

$$S_{q,B}(\omega) = \frac{S_{f,\mathrm{bu}}(\omega)}{(k_s\mathcal{K}(\omega))^2} \tag{13}$$

and the corresponding variance is expressed as a function of the filtered variance of the buffeting load

$$\sigma_{q,B}^2 = \frac{1}{k_s^2}\int_{-\infty}^{+\infty}\frac{S_{f,\mathrm{bu}}(\omega)}{\mathcal{K}^2(\omega)}\mathrm{d}\omega. \tag{14}$$

In this expression, $1/\mathcal{K}(\omega)$ can be seen as a frequency response function filtering out the frequency content of the buffeting loading. Since the timescales in $\mathcal{K}(\omega)$ and $S_{f,\mathrm{bu}}(\omega)$ might be similar, it is not possible to further simplify this expression. It constitutes the *background* component of the response. Notice that under the quasi-steady assumption, $\mathcal{K}(\omega) \to 1$ and (14) degenerates into the usual background component.

3.3. The resonant component

In the variance of the response, defined in (7), the background component is trivially added and subtracted. This yields

$$\sigma_q^2 = \sigma_{q,\mathrm{B}}^2 + \int_{-\infty}^{+\infty}\left[S_q(\omega) - S_{q,\mathrm{B}}(\omega)\right]\mathrm{d}\omega. \tag{15}$$

The resonant component is then readily identified, as the main component in the residue $S_{q,1}(\omega) := S_q(\omega) - S_{q,\mathrm{B}}(\omega)$, which is also written

$$S_{q,1}(\omega) = \left(|H(\omega)|^2 - \frac{1}{(k_s\mathcal{K}(\omega))^2}\right)S_{f,\mathrm{bu}}(\omega) \tag{16}$$

Indeed, the main contribution to this residue amounts from the two resonance peaks of the aeroelastic system located in $\pm\overline{\omega}$. Assuming small damping (Assumption (ii)), the resonance frequency of the aeroelastic system is defined by

$$-\frac{\overline{\omega}^2}{\omega_s^2} + \mathcal{K}(\overline{\omega}) = 0, \tag{17}$$

which is the pole of the frequency response function $H(\omega)$ for negligible damping ratio, see (12). Dropping higher order terms, the resonance frequency is therefore defined by $\mathcal{K}(\overline{\omega}) = \overline{\omega}^2/\omega_s^2$. This equation is not difficult to solve; it is nothing but a nonlinear eigenvalue problem. In this SDOF case, it turns into a nonlinear algebraic equation. The unicity of the solution is not guaranteed, multiple poles might arise. Solutions can be built by continuation as detailed next. We can also notice that $\overline{\omega}$ is the solution of a problem that is independent of ξ_s. It is therefore independent of the perturbation analysis.

Considering now that $\overline{\omega}$ is known (for a given wind velocity), a stretched coordinate η is introduced to zoom on the resonance peak in the neighborhood of $\omega = +\overline{\omega}$. This is formally written

$$\omega = \overline{\omega}(1 + \xi_s\eta), \tag{18}$$

where $\eta = \mathcal{O}(1)$. Assuming now that $\mathcal{K}$ and $\mathcal{C}$ are smooth functions in the neighborhood of $\overline{\omega}$ (Assumption (iii)), they can be expanded as

$$\mathcal{K}(\omega) = \mathcal{K}(\overline{\omega}) + \xi_s\eta\,\overline{\omega}\partial_\omega\mathcal{K}(\overline{\omega}) + \mathcal{O}(\xi_s^2), \tag{19}$$

$$\mathcal{C}(\omega) = \mathcal{C}(\overline{\omega}) + \xi_s\eta\,\overline{\omega}\partial_\omega\mathcal{C}(\overline{\omega}) + \mathcal{O}(\xi_s^2), \tag{20}$$

which can be truncated at order ξ_s provided higher order derivatives are small enough to keep the asymptoticness of this series ($\xi_s^i\overline{\omega}^i\partial_\omega^i\mathcal{K}(\overline{\omega}) \ll \mathcal{K}(\overline{\omega})$).

Substituting (18), (19) and (20) into the frequency response function (12) leads to

$$H[\omega(\eta)] = \frac{1}{k_s}\Bigg[-\frac{\overline{\omega}^2}{\omega_s^2}(1+\xi_s\eta)^2 + 2\mathrm{i}\xi_s\frac{\overline{\omega}}{\omega_s}(1+\xi_s\eta)(\mathcal{C}(\overline{\omega}) + \xi_s\eta\,\overline{\omega}\partial_\omega\mathcal{C}(\overline{\omega})) + \mathcal{K}(\overline{\omega}) + \xi_s\eta\,\overline{\omega}\partial_\omega\mathcal{K}(\overline{\omega}) + \mathcal{O}(\xi_s^2)\Bigg]^{-1} \tag{21}$$

or, collecting the likewise powers of ξ_s together,

$$H[\omega(\eta)] = \frac{1}{k_s}\Bigg[\left(\mathcal{K}(\overline{\omega}) - \frac{\overline{\omega}^2}{\omega_s^2}\right) + \left(-2\eta\frac{\overline{\omega}^2}{\omega_s^2} + 2\mathrm{i}\frac{\overline{\omega}}{\omega_s}\mathcal{C}(\overline{\omega}) + \overline{\omega}\partial_\omega\mathcal{K}(\overline{\omega})\eta\right)\xi_s + + \left(-\eta^2\frac{\overline{\omega}^2}{\omega_s^2} + 2\mathrm{i}\frac{\overline{\omega}}{\omega_s}(\mathcal{C}(\overline{\omega}) + \overline{\omega}\partial_\omega\mathcal{C}(\overline{\omega}))\eta\right)\xi_s^2 + +\mathcal{O}(\xi_s^3)\Bigg]^{-1}. \tag{22}$$

Remembering the definition (17) of $\overline{\omega}$, it is readily seen that the first term drops so that the leading term in the brackets is in ξ_s. It is then decided to truncate the series at order ξ_s, invoking Assumption (ii) again. The frequency response function is therefore expressed, at leading order,

$$H(\omega(\eta)) = \frac{1}{2\xi_s k_s}\left[\left(-\frac{\overline{\omega}^2}{\omega_s^2} + \frac{1}{2}\overline{\omega}\partial_\omega\mathcal{K}(\overline{\omega})\right)\eta + \mathrm{i}\frac{\overline{\omega}}{\omega_s}\mathcal{C}(\overline{\omega})\right]^{-1}. \tag{23}$$

This expression recalls the formulation for a classical single degree-of-freedom system (see Example 1). It captures the order of magnitude of the resonance peak, $\frac{1}{2k_s\xi_s}$ and, at the same time, accounts for the frequency-dependent nature of the stiffness and viscosity. The asymptotic analysis that has been performed so far assumes that all quantities other than ξ_s are of order 1. As seen in (23), the frequency response function of the aeroelastic system is expressed as a function of the aerodynamic stiffness $\mathcal{K}(\overline{\omega})$ which enters in the definition of $\overline{\omega}$, the aerodynamic viscosity $\mathcal{C}(\overline{\omega})$ and the gradient of the aerodynamic stiffness $\partial_\omega\mathcal{K}(\overline{\omega})$ in the neighborhood of the resonance peak. This is precisely to account for the possible non negligible variation of the aerodynamic stiffness across the width of the resonance peak. At leading order, and assuming that $\partial_\omega\mathcal{C}(\overline{\omega})\tilde{}1$, this expression also shows that the gradient in the viscosity $\partial_\omega\mathcal{C}(\overline{\omega})$ is actually repelled to a higher order; this is a consequence of the assumption of small damping ratio. Nevertheless if $\partial_\omega\mathcal{C}(\overline{\omega})$ was much larger than 1, which is a case we have not encountered in the applications

that have been studied so far, it could be possible to enrich the proposed approximation. This approach is summarized in Appendix A, where both the derivatives of $\mathcal{K}(\overline{\omega})$ and $\mathcal{C}(\overline{\omega})$ are included in the approximation.

The substitution of (23) (which is of order $1/\xi_s$) into (16) indicates that the term $1/(k_s\mathcal{K}(\omega))^2$ can be neglected, so that the residue is given by

$$\hat{S}_{q,1}(\omega(\eta)) = \frac{S_{f,\mathrm{bu}}(\omega(\eta))}{(2k_s\xi_s)^2} \frac{1}{\left(\frac{\overline{\omega}^2}{\omega_s^2} - \frac{1}{2}\overline{\omega}\partial_\omega\mathcal{K}(\overline{\omega})\right)^2\eta^2 + \left(\frac{\overline{\omega}}{\omega_s}\mathcal{C}(\overline{\omega})\right)^2}. \tag{24}$$

It is also usual to assume that the power spectral density of the buffeting loading does not vary too fast in the neighborhood of the resonance peak —other solutions are available otherwise—, *i.e.* $S_{f,\mathrm{bu}}(\omega(\eta)) = S_{f,\mathrm{bu}}(\overline{\omega}) + \mathcal{O}(\xi_s)$. In this case, this term is seen as a constant with respect to integration along ω. The resonant component is obtained by multiplying $\hat{S}_{q,1}(\omega(\eta))$ by 2 in order to take into account the two resonance peaks located at $\omega = \pm\overline{\omega}$, and integrating along frequencies

$$\sigma_{q,\mathrm{R}}^2 = 2\int_0^{+\infty} \hat{S}_{q,1}(\omega(\eta))\xi_s\overline{\omega}\mathrm{d}\eta. \tag{25}$$

This integral accepts a closed form expression since the PSD of the loading is replaced by $S_{f,\mathrm{bu}}(\overline{\omega})$. After substitution of (24) into (25) and some standard calculus, the resonant component is finally given by

$$\sigma_{q,\mathrm{R}}^2 = \frac{S_{f,\mathrm{bu}}(\overline{\omega})}{k_s^2}\frac{\pi\omega_s}{2\xi_s\mathcal{C}(\overline{\omega})}\frac{1}{\left|\frac{\overline{\omega}^2}{\omega_s^2} - \frac{\overline{\omega}\partial_\omega\mathcal{K}(\overline{\omega})}{2}\right|}. \tag{26}$$

Returning to original variables, the resonant contribution is expressed under a generalized form of the well known resonant contribution for systems with constant mechanical properties,

$$\sigma_{q,\mathrm{R}}^2 = \frac{S_{f,\mathrm{bu}}(\overline{\omega})}{k_s^2}\frac{\pi\omega_s}{2\xi_s}\frac{c_s}{c_s - c_{\mathrm{ae}}(\overline{\omega})}\frac{k_s}{\left|k_s - k_{\mathrm{ae}}(\overline{\omega}) + \frac{1}{2}\overline{\omega}\partial_\omega k_{\mathrm{ae}}(\overline{\omega})\right|}. \tag{27}$$

The last two factors are indeed equal to 1 in the absence of aerodynamic stiffness and viscosity. When these quantities are not null, the damping ratio of the system is affected and is not equal to the structural damping ratio. This justifies the introduction of a new damping ratio that includes the aeroelastic contribution

$$\overline{\xi} := \frac{c_s - c_{\mathrm{ae}}(\overline{\omega})}{2\sqrt{(k_s - k_{\mathrm{ae}}(\overline{\omega}))m_s}}. \tag{28}$$

The substitution in (27) ultimately yields

$$\sigma_{q,\mathrm{R}}^2 = \frac{S_{f,\mathrm{bu}}(\overline{\omega})}{(k_s - k_{\mathrm{ae}}(\overline{\omega}))^2}\frac{\pi\overline{\omega}}{2\overline{\xi}}\frac{1}{1 + \frac{1}{2}\frac{\overline{\omega}\partial_\omega k_{\mathrm{ae}}(\overline{\omega})}{k_s - k_{\mathrm{ae}}(\overline{\omega})}}$$

which makes it even more obvious that this is a generalization of the well-known (B/R), to systems with smoothly varying mechanical properties, while the smoothly varying buffeting spectra is handled in the same convenient manner as in the original decomposition.

3.4. Summary with dimensional quantities and practical implementation

The addition of the background component to the resonant one provides

$$\sigma_q^2 = \sigma_{q,\mathrm{B}}^2 + \frac{S_{f,\mathrm{bu}}(\overline{\omega})}{(k_s - k_{\mathrm{ae}}(\overline{\omega}))^2}\frac{\pi\overline{\omega}}{2\overline{\xi}}\frac{1}{1 + \frac{1}{2}\frac{\overline{\omega}\partial_\omega k_{\mathrm{ae}}(\overline{\omega})}{k_s - k_{\mathrm{ae}}(\overline{\omega})}}, \tag{29}$$

where in the dimensional version, the eigenvalue of the aeroelastic system is computed by

$$k_s - k_{\mathrm{ae}}(\overline{\omega}) - m_s\overline{\omega}^2 = \mathrm{ord}(\xi_s). \tag{30}$$

In practice, the flutter analysis is repeated for several increasing values of the wind speed $\{U^{(n)}\}$, $n \in \mathbb{N}$, starting from $U^{(0)} = 0$ m/s and until a critical state is reached. For each increment in this sequence, a simple iterative method, based on the power method, can be used to compute $\overline{\omega}(U^{(n)})$. Starting from the first guess $\overline{\omega}_{(0)} = \overline{\omega}(U^{(n-1)})$, or $\overline{\omega}_{(0)} = \omega_s$ when $n = 0$, just a couple of iterations can be performed at each increment of wind speed in order to converge to the new natural frequency. The iterative scheme is as simple as

$$\overline{\omega}_{(i+1)} = \sqrt{\frac{k_s - k_{\mathrm{ae}}(\overline{\omega}_{(i)})}{m_s}}. \tag{31}$$

where $k_{\mathrm{ae}}(\overline{\omega}_{(i)})$ is the aerodynamic stiffness corresponding to the frequency $\overline{\omega}_{(i)}$ and wind velocity $U^{(n)}$. This operation is repeated a couple of times until a desired convergence criterion is reached and $\lim_{i\to+\infty}\overline{\omega}_{(i+1)} = \overline{\omega}(U^{(n)})$. At this stage, it is recalled that the analysis is performed for $U \le U_{\mathrm{div.}}$ so that $k_s - k_{\mathrm{ae}}(\overline{\omega}_{(i)})$ is indeed positive.

In the pitch-plunge model (Bisplinghoff and Ashley, 2013), the aerodynamic forces per unit length are expressed as

$$\begin{pmatrix} L_{\mathrm{se}}(\omega) \\ M_{\mathrm{se}}(\omega) \end{pmatrix} = q\left(\frac{\omega B}{U}\right)^2\begin{pmatrix} 1 & 0 \\ 0 & B \end{pmatrix}\begin{bmatrix} \mathrm{H}_1^*\mathrm{i} + H_4^* & \mathrm{H}_2^*\mathrm{i} + H_3^* \\ A_1^*\mathrm{i} + A_4^* & A_2^*\mathrm{i} + A_3^* \end{bmatrix}\begin{Bmatrix} Z(\omega) \\ B\Theta(\omega) \end{Bmatrix} \tag{32}$$

where $q = \frac{1}{2}\rho U^2$, H_i^* and A_i^* for $i = \{1, .., 4\}$ are the flutter derivatives of the deck cross section according to the Scanlan formulation, U is the average wind velocity, B is the width of the deck and ρ is the density of the air. According to Davenport's model (Davenport, 1962), the buffeting forces are defined by

$$\begin{pmatrix} L_{\mathrm{bu}}(\omega) \\ M_{\mathrm{bu}}(\omega) \end{pmatrix} = \frac{qB}{U}\begin{bmatrix} 2\pi A(\omega) \\ \frac{\pi}{2}BA(\omega) \end{bmatrix}W(\omega), \tag{33}$$

where $A(\omega)$ is the real function called admittance, that weights the quasi-steady values of buffeting forces in the frequency domain and $W(\omega)$ is the Fourier transform of the vertical wind velocity $w(t)$. This formulation and these notations are similar to common practice in the field, see e.g. (Diana et al., 2019). In this paper, a single degree-of-freedom model is considered. Keeping only the rotational degree-of-freedom, the equation of motion governing stall flutter is obtained

$$\left(-\omega^2 I_s + 2\xi I_s\omega_s(\mathrm{i}\omega) + I_s\omega_s^2\right)\Theta(\omega) = M_{\mathrm{se}}(\omega) + M_{\mathrm{bu}}(\omega), \tag{34}$$

where I_s is the mass moment of inertia per unit length and such that the aeroelastic pitching moment and the buffeting pitching moment are reduced to

$$\begin{aligned} M_{\mathrm{se}}(\omega) &= qB^2\left(\frac{\omega B}{U}\right)^2\left(A_2^*\mathrm{i} + A_3^*\right)\Theta(\omega), \\ M_{\mathrm{bu}}(\omega) &= \frac{qB}{U}\left(\frac{\pi}{2}BA(\omega)\right)W(\omega) \end{aligned} \tag{35}$$

On account that $M_{\mathrm{se}}(\omega) = (\mathrm{i}\omega c_{\mathrm{ae}}(\omega) + k_{\mathrm{ae}}(\omega))\Theta(\omega)$, comparison with (4) shows that

$$\begin{aligned} k_{\mathrm{ae}}(\omega) &= qB^2\left(\frac{\omega B}{U}\right)^2 A_3^*(\omega), \\ c_{\mathrm{ae}}(\omega) &= qB^2\frac{B}{U}\left(\frac{\omega B}{U}\right)A_2^*(\omega) \end{aligned} \tag{36}$$

These latter equations will serve as common basis for all the following illustrations. In these illustrations, the proposed extension of the B/R decomposition will be used to compute the standard deviation of the torsional response; it will also be compared to an accurate result obtained

by numerical integration of the power spectral density of the response.

4. Illustrations

4.1. Illustration 1 - application to bluff bodies

For this first illustration, the B/R decomposition is applied to the Golden Gate and Tacoma Narrows bridges. For both structures, the flutter derivatives $A_2^*(\omega)$ and $A_3^*(\omega)$ shown in Fig. 2 as well as other useful data summarized in Table 1 are considered. These values are taken from (Canor et al., 2015; Foucriat and Cremona, 2002; Larsen, 2000; Larsen, 1998). The aerodynamic stiffness and viscosity $k_{ae}(\omega)$ and $c_{ae}(\omega)$ are obtained with (36) and spline interpolation.

To ensure a safe behavior against flutter, the variance of the torsional displacement must be calculated for a sufficiently wide range of wind velocities U. The results obtained for the Golden Gate Bridge are shown in Fig. 3. The power spectral density of the torsional response is shown in Fig. 3-a for several values of U. The exact power spectral density is compared to the power spectral density corresponding to the B/R decomposition (in a log scale). The agreement is very good where the power spectral densities are large. This is also confirmed on Fig. 3-b showing the variance of the torsional response., the proposed method shows a perfect superposition with the reference curve obtained from numerical integration, until the critical wind velocity $U_{cr} \approx 24$ m/s, represented by the dashed line and evaluated with (8). The background (B) contribution to the displacement standard deviation is very low and a quite accurate expression can already be obtained from the resonant component (R) alone. This is justified by the fact that this first illustration corresponds to a torsional galloping, as clearly illustrated from the power spectral densities: the frequency is not affected by the wind velocity but the damping ratio drops to zero when approaching the critical wind velocity. The relative error on the numerically integrated curve does not exceed 1% as illustrated by 3-e. Also, the magnitude of the aeroelastic damping and stiffness gradients $\partial_\omega \mathcal{K}(\overline{\omega})$ and $\partial_\omega \mathcal{C}(\overline{\omega})$, plotted as a function of U in 3-c, validates the truncation of the series expansions (19 and 20). Finally, it is observed in Fig. 3-d that the structure indeed fails from a galloping instability, since the damping becomes negative at the critical velocity U_{cr}. The value obtained for the critical velocity is corroborated by (Canor et al., 2015), and matches well the vertical asymptote of the standard deviation of the torsional displacement.

The second example, the first Tacoma Narrows bridge, is widely known for its unstable flutter behavior (Larsen, 2000). The results obtained for this second example are shown in Fig. 4. Globally, the structural behavior is very similar to the one previously discussed, but the critical speed is significantly lower. The instability corresponds again to a torsional galloping. It takes place at a wind velocity of 11.5 m/s, which is

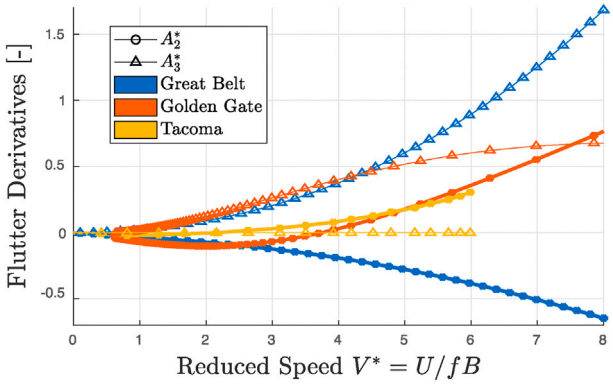

Fig. 2. Flutter derivatives $A_2^*(\omega)$ and $A_3^*(\omega)$ of the structures considered in Illustrations 1 and 2.

Table 1
Structural properties of the structures considered in Illustrations 1 and 2.

	Golden Gate	Tacoma	Storebaelt
Moment of Inertia I_s [kg/m]	$4.4 \cdot 10^6$	$177.73 \cdot 10^3$	$2.47 \cdot 10^6$
Natural frequency f_s [Hz]	0.1916	0.20	0.278
Damping Ratio ξ_s [%]	0.5	0.5	0.3
Deck width B [m]	27.43	12.0	31
Aeroelastic Model	Bluff body	Bluff body	Flat Plate
Type of instability	Galloping	Galloping	Divergence

consistently obtained either with formula (8) giving the critical wind velocity, either by reproducing the complete flutter response $\sigma_\theta(U)$, or when the damping ratio $\overline{\xi}(U)$ estimated with the proposed method reaches zero. It is also consistent with the values provided in (Larsen, 1998). More importantly, the complete flutter response is again accurately captured by the proposed extension of the B/R decomposition; yet, the resonant part of the response is seen to be the most important.

4.2. Illustration 2 - application to the flat plate model

The next example is borrowed from the recent benchmark about flutter analysis of bridges (Diana et al., 2019). In that benchmark, a pitch/plunge model of the Storebaelt bridge is studied with the actual structural properties of the bridge and with the aerodynamic properties of a flat plate (Theodorsen, 1935). In this paper, we further reduce this study to the sole torsional dynamics. The aeroelastic deck section is idealized by a flat plate, a simplification which is known to be useful in the prediction of more complex geometries (Caracoglia and Jones, 2003).

The flutter derivatives are expressed as functions of $F(\omega)$ and $G(\omega)$, respectively the real and imaginary part of Theodorsen's circulation complex function $C(\omega)$. This function considers the non-stationary contribution through the fluid-structure interaction. The function is approximated by the analytical formula suggested by (Jones, 1940), that involves a combination of exponential functions. This approximation is used in the following developments.

The flutter derivatives $A_2^*(\omega)$ and $A_3^*(\omega)$ read (Diana et al., 2019)

$$\begin{aligned} A_2^*(\omega) &= -\frac{\pi}{8}\frac{U}{\omega B}\left(1 - F(\omega) - \frac{4U}{\omega B}G(\omega)\right), \\ A_3^*(\omega) &= \frac{\pi}{2}\left(\frac{U}{\omega B}\right)^2\left(F(\omega) - \frac{\omega B}{4U}G(\omega)\right) \end{aligned} \tag{37}$$

so that the aeroelastic stiffness and damping obtained by (36) read

$$\begin{aligned} k_{ae} &= qB^2\frac{\pi}{2}\left(F(\omega) - \frac{\omega B}{4U}G(\omega)\right) \\ c_{ae} &= -q\frac{B^3}{U}\frac{\pi}{8}\left(1 - F(\omega) - \frac{4U}{\omega B}G(\omega)\right) \end{aligned} \tag{38}$$

Before tackling the analysis, it is possible to predict the type of instability based on the knowledge of the flutter derivatives. As shown in Fig. 2, the damping-related flutter derivative A_2^* is negative, whereas the stiffness-related flutter derivative A_3^* is positive. In other terms, the aeroelastic loading provides additional damping to the structure, while it decreases the total aeroelastic stiffness. Accordingly, the bridge heads towards a divergence instability.

This is confirmed by Fig. 5-d, showing a natural frequency decreasing with the wind velocity. Fig. 5-d also reveals a marked grow of the total damping ratio $\overline{\xi}$ for increasing velocity, reaching more than 20% for wind velocities larger than 80 m/s, going therefore beyond the scope of assumption (i). Even so, the proposed analytical solution remains in good agreement with numerical results for small to intermediate values of velocity U, as shown in Fig. 5-b. As a matter of fact, the power spectral densities and standard deviations are well approximated, with acceptable errors (<10%) up to a wind velocity of 80 m/s. In the proposed method,

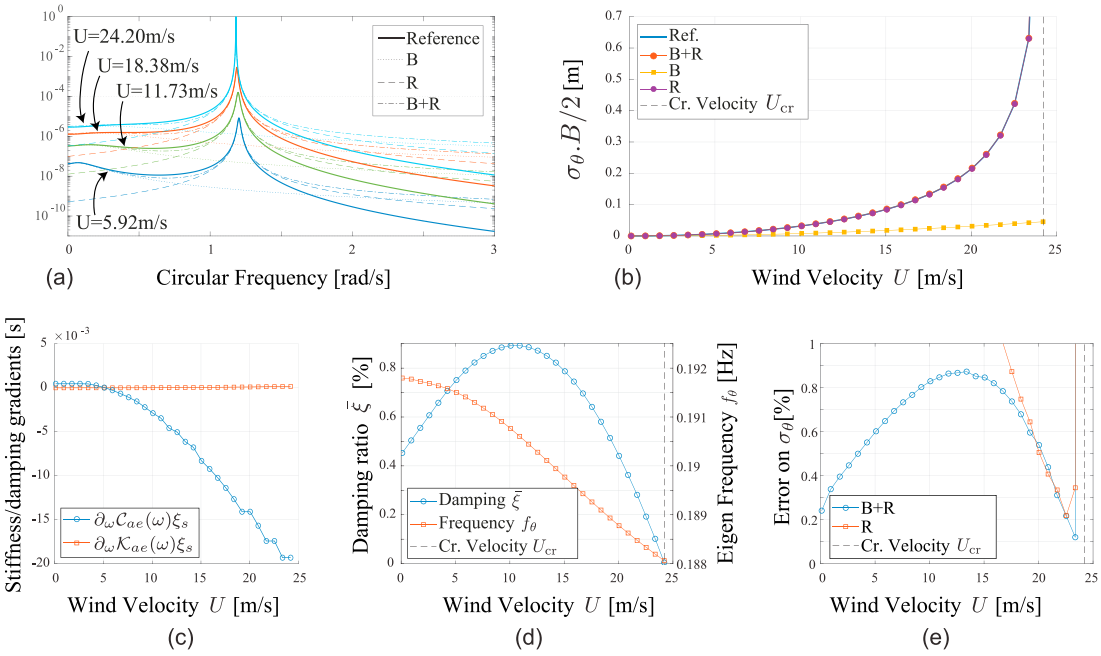

Fig. 3. Results obtained from background/resonant methods applied to the first illustration (Golden Gate Bridge). (a) PSD and their approximations for different wind velocities. (b) Scaled standard deviations obtained from background component (B), resonant components (R), and the sum of them (B)+(R). (c) Evolution of scaled aeroelastic stiffness and damping gradients with respect to avg. wind velocity. (d) Damping ratio at resonance with respect to avg. wind velocity. (e) Error on σ_θ with respect to avg. wind velocity.

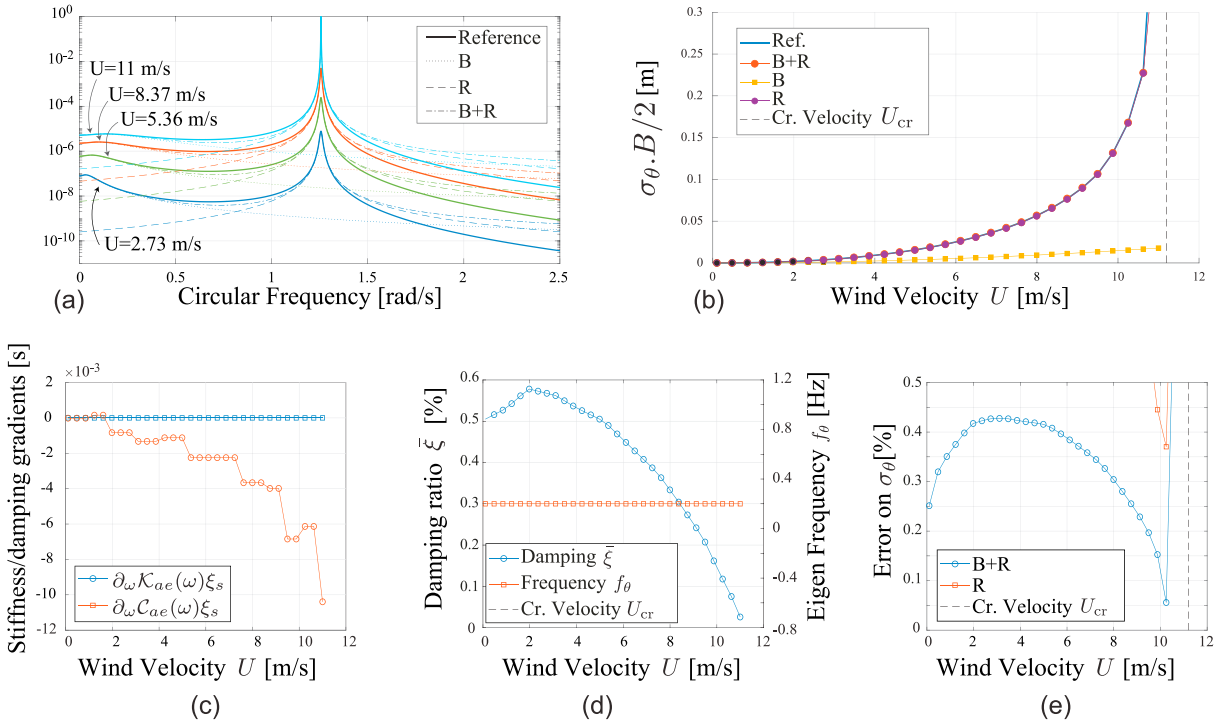

Fig. 4. Results obtained from background/resonant methods applied to the first illustration (Tacoma Narrows bridge). (a) PSD and their approximations for different wind velocities. (b) Scaled standard deviations obtained from background component (B), resonant components (R), and the sum of them (B)+(R). (c) Evolution of scaled aeroelastic stiffness and damping gradients with respect to avg. wind velocity. (d) Damping ratio at resonance with respect to avg. wind velocity. (e) Error on σ_θ with respect to avg. wind velocity.

the order of magnitude of the error corresponds to the total damping ratio $\bar{\xi}$; in this example, the total damping ratio reaches 20% around 80 m/s which matches the order of magnitude of the error of 10% (the proposed method is therefore more relevant when the instability occurs in galloping-type rather than divergence-type instability). Beyond this point, a lack of precision shows up right before the vertical asymptote defining the critical velocity, where a larger discrepancy appears with respect to the numerical solution. Given the magnitude of the damping in

this range of velocity, the eigenvalue problem (30) needs to be reconsidered by including the damping ratio at leading order.

4.3. Illustration 3 - torsional galloping of a bridge deck section of the Third Bosphorus bridge during lifting operations

This application presents a real torsional SDOF model behavior. During the Third Bosphorus bridge deck building operations, each segment of the deck was positioned by lifting from a floating platform to the deck level, at a height of 75 m above sea level, see Fig. 6-a. This operation involves a 825 t load to be lifted and last sufficiently long for the deck segment to be submitted to turbulent winds and possible aeroelastic instability (Andrianne and de Ville de Goyet, 2016). This system is particularly compliant in torsion along the vertical axis, as the strandjacks are relatively close to each other. In these circumstances, the deck segment is highly sensitive to aeroelastic instabilities and, if no precaution is taken, torsional galloping could be observed with angular displacements larger than 30° in most severe configurations.

Each deck segment is characterized by a mass $m_s = 825$ t, a width $B = 58.4$ m, and a length $D = 14$ m, see Fig. 6-a. The strandjacks are separated by 6 m × 13.5 m, and the modal parameters are shown in Table 2. The stiffness in torsion is calculated by

$$k_\theta = \frac{m_s g d^2}{L},$$

where g is the acceleration of gravity, $L \in \{0, 100\}$ m is the length of the lifting cables and $d = 7.4$ m the distance from the strandjacks to the center of rotation of the segment. This stiffness is computed from the pendulum-like stiffness $m_s g/L$ of a single cable; for a unit rotation of the deck, $\theta = 1$, the displacement of the anchorages is equal to d which gives after multiplication by the pendulum-like stiffness and the lever arm d, the torsional moment corresponding to a unit rotation. The Scanlan derivatives have been determined by experimental testing at the University of Liège (Andrianne and de Ville de Goyet, 2016); this study has revealed that the wind velocity does not affect the eigen frequency and thus, the stiffness. The derivative A_3^* is therefore negligible. The structural properties are summarized in Table 2, and the only remaining flutter derivative of interest, A_2^*, is shown in Fig. 6-b as a function of the reduced frequency $U/fB = 2\pi U/\omega B$. Following the quasi-steady theory, the buffeting forces are described by

$$F_b = \left(\frac{1}{2}\rho U B \frac{dC_M}{d\beta}\right)^2 S_w(\omega), \tag{39}$$

where $dC_M/d\beta = -0.02$ is the derivative of the moment coefficient with respect to the torsional coordinate β. This value has been determined with stationary tests on a rigid bridge deck segment mounted on a high frequency force balance at the University of Liège; it is also consistent with the torsional coefficients measured on cantilever bridges under construction (Pindado et al., 2005).

The analysis is repeated for several values of wind velocity up to critical state as shown in Fig. 7. The superimposed power spectral densities of Fig. 7-a are fully centered on 0.18 Hz, showing that no frequency shifting occurs with increasing incoming wind speed, due to the negligible aeroelastic stiffness. Therefore this is an example of pure torsional galloping. Because the scaled damping gradient $\partial_\omega \mathcal{C}(\overline{\omega})\xi_s\overline{\omega}$ is of order 10^{-3}, its contribution to the transfer function is of order 10^{-6} and can clearly be neglected in front of $\mathcal{O}(\xi_s)$ terms, as it was assumed in (23). Again, the background resonant decomposition provides an excellent estimation of the standard deviation of the torsional coordinate, with a relative error constantly lower than 0.3%. The vertical asymptote in the neighborhood of the critical regime takes place around 12 m/s, which is also the velocity at which the aeroelastic damping equals the structural damping, see Fig. 7-d; this is also consistent with available results in the literature (Andrianne and de Ville de Goyet, 2016).

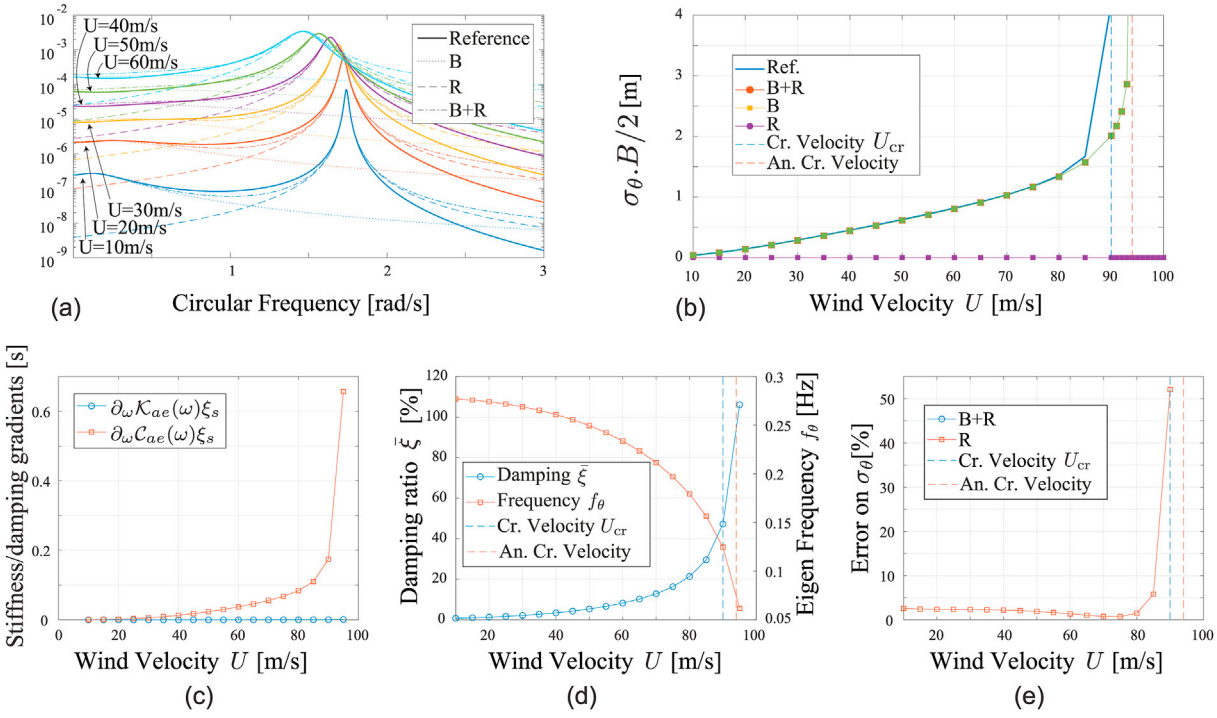

Fig. 5. Results obtained from background/resonant methods applied to the first illustration (Great Belt Bridge). (a) PSD and their approximations for different wind velocities. (b) Scaled standard deviations obtained from background component (B), resonant component (R), and from combinations of them. (c) Scaled aeroelastic stiffness and damping gradients evolution with respect to avg. wind velocity. (d) Damping ratio at resonance with respect to avg. wind velocity. (e) Error on σ_θ with respect to avg. wind velocity.

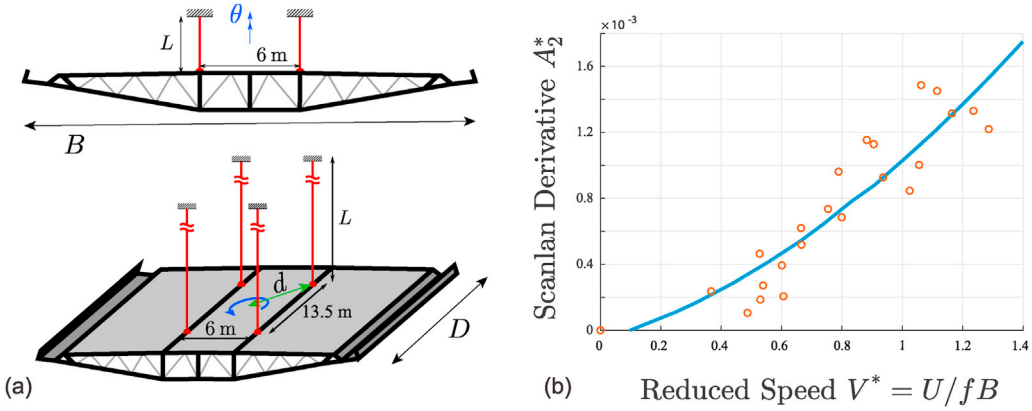

Fig. 6. (a) View of the deck segment during lifting operation, (b) Flutter derivatives $A_2^*(\omega)$ and $A_3^*(\omega)$ of the Third Bosphorus bridge deck segment (both experimental data and fitting are taken from (Andrianne and de Ville de Goyet, 2016)).

Table 2
Modal parameters for the segment deck during lifting operation.

	Segment BB3
Cable length L [m]	100
Torsional radius d [m]	7.39
Segment mass m_s [kg]	$8.25 \cdot 10^5$
Eigen Frequency f_s [m]	0.031
Damping Ratio ξ_s [%]	0.2
Type of instability	Galloping

5. Conclusion

The complete flutter analysis of a structure requires the repeated analysis of the aeroelastic response of the structure for various wind velocities. Each of these analyses is based on the integration of the power spectral density of the aeroelastic response. Traditional integration methods struggle to efficiently estimate these integrals because of the marked peakedness of the function in the neighborhood of the poles of the system. In this paper, we have derived an extension of the Background/Resonant decomposition (which is commonly applied under the quasi-steady assumption), to aeroelastic analysis, where the stiffness and damping of the coupled system change with frequency.

Assuming significantly different timescales in the buffeting loading and in the natural frequencies of the aeroelastic system, a small damping ratio ξ_s, and smoothly varying aeroelastic stiffness and damping, we have derived a closed form expression for the variance of the response as a sum of a Background and a Resonant components. This result has been obtained by specializing the more general framework known as Multiple Timescale Spectral Analysis. It is shown that the background component takes a slightly different form than usual, since the energy of the buffeting loading is lowpass filtered and not just translated in a quasi-static manner. Also the resonant component assumes a form that is very similar to the classical decomposition, with the differences that the quantities

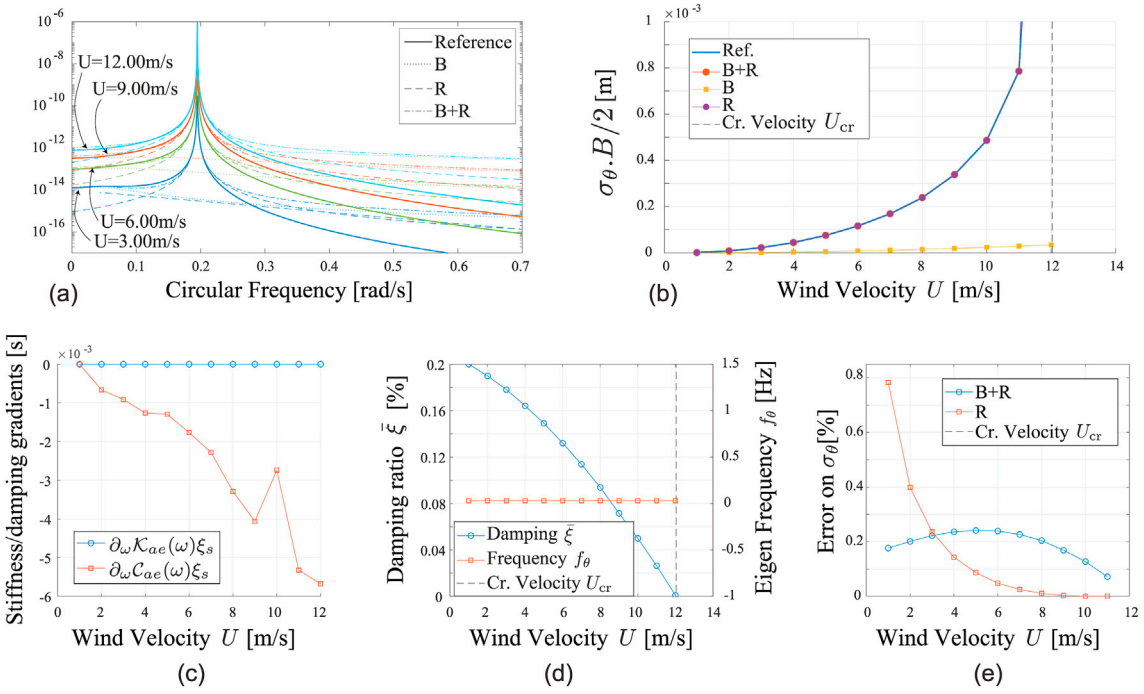

Fig. 7. Results obtained from background/resonant methods applied to the third illustration (Bosphorus Bridge deck segment). (a) PSD and their approximations for different wind velocities. (b) Scaled standard deviations obtained from background component (B), resonant components (R), and the sum of them (B)+(R). (c) Evolution of scaled aeroelastic stiffness and damping gradients with respect to avg. wind velocity. (d) Damping ratio at resonance with respect to avg. wind velocity. (e) Error on σ_θ with respect to avg. wind velocity.

related to the natural frequency of the structural system are moved to the natural frequency of the aeroelastic system and that there is an additional coefficient in the expression, taking care of the possible non negligible change of the aeroelastic stiffness in the neighborhood of the natural frequency of the aeroelastic system.

The proposed method is tested on three realistic examples. It has shown accurate results with an error lower than 1% in most cases. Torsional galloping is accurately captured since it meets the assumptions of the model; torsional divergence of the flat plate is also well represented but until approximately 90% of the critical wind velocity since the damping ratio is too large beyond that point.

This extension of the background/resonant decomposition to SDOF aeroelastic systems with frequency dependent stiffness and viscosity is successful. It might seem at this stage of minor interest since the domain of application does not require heavy calculation power. However, it shall constitute a major cornerstone of the extension of the method to MDOF systems for which the computation load remains critical. Analytical solution, although approximate at some point, also offer a better understanding of the different contributions to the integral.

CRediT authorship contribution statement

Julien Heremans: Writing - original draft, preparation, Investigation, Software, Validation, Data curation, Visualization. **Anass Mayou:** Software, Validation, Visualization, Writing - review & editing. **Vincent Denoël:** Writing - original draft, preparation, Conceptualization, Methodology, Writing - review & editing.

Declaration of competing interest

The authors declare that they have no known competing financial interests or personal relationships that could have appeared to influence the work reported in this paper.

Appendix

The derivation of the first order approximation for $H(\omega)$ was obtained in (23) truncating (22) at leading order. If it is clear that $\overline{\omega}/\omega$ and $\mathcal{C}(\omega) = 1 - c_{ae}(\omega)/c_s$ are of order $\mathcal{O}(1)$, the magnitude of $\partial_\omega C(\overline{\omega})$ is less easily predicted, and some applications could potentially embed a large damping gradient, especially if they are subjected to galloping instabilities, where the damping could vary rapidly. This section details this uncovered particular case of a large $\partial_\omega \mathcal{C}(\overline{\omega})$. Restarting from (22) and remembering the definition (17) of $\overline{\omega}$

$$H[\omega(\eta)] = \frac{1}{k_s}\left[\left(-2\eta\frac{\overline{\omega}^2}{\omega_s^2} + 2\mathrm{i}\frac{\overline{\omega}}{\omega_s}\mathcal{C}(\overline{\omega}) + \overline{\omega}\partial_\omega \mathcal{K}(\overline{\omega})\,\eta\right)\xi_s + \left(-\eta^2\frac{\overline{\omega}^2}{\omega_s^2} + 2\mathrm{i}\frac{\overline{\omega}}{\omega_s}(\mathcal{C}(\overline{\omega}) + \overline{\omega}\partial_\omega \mathcal{C}(\overline{\omega}))\eta\right)\xi_s^2 + +\mathcal{O}(\xi_s^3)\right]^{-1}.$$

Assuming now that $\partial_\omega C(\overline{\omega})$ is of order $\mathcal{O}\left(\frac{1}{\xi_s}\right)$, and truncating at leading order,

$$H(\omega(\eta)) = \frac{1}{2\xi_s k_s}\left[\left(-\frac{\overline{\omega}^2}{\omega_s^2} + \frac{1}{2}\overline{\omega}\partial_\omega \mathcal{K}(\overline{\omega})\right)\eta + \mathrm{i}\frac{\overline{\omega}}{\omega_s}\eta\,\overline{\omega}\partial_\omega \mathcal{C}(\overline{\omega})\xi_s\right]^{-1}. \tag{40}$$

This expression generalizes (23) to large damping gradient. Since $H(0)$ is still asymptotic to $1/k_s\mathcal{K}(\omega)$, the background component remains unchanged, and the resonant component only deserves further study.

In (24), the residue is approached by

$$\hat{S}_{q,1}(\omega(\eta)) = \frac{1}{(2k_s\xi_s)^2}\frac{1}{\alpha\eta^2 + \beta\eta + \gamma}S_{f,\mathrm{bu}}(\omega(\eta)) \tag{41}$$

with

$$\alpha = \left(\frac{\overline{\omega}^2}{\omega_s^2} - \frac{1}{2}\overline{\omega}\partial_\omega \mathcal{K}(\overline{\omega})\right)^2 + \xi_s^2\left(\frac{\overline{\omega}}{\omega_s}\right)^2(\overline{\omega}\partial_\omega \mathcal{C}(\overline{\omega}))^2,$$

$$\beta = 2\xi_s\left(\frac{\overline{\omega}}{\omega_s}\right)^2\mathcal{C}(\overline{\omega})\overline{\omega}\partial_\omega \mathcal{C}(\overline{\omega})$$

$$\gamma = \left(\frac{\overline{\omega}}{\omega_s}\mathcal{C}(\overline{\omega})\right)^2.$$

Again, we assume that the power spectral density of the buffeting loading does not vary too fast in the neighborhood of the resonance peak such that $S_{f,\mathrm{bu}}(\omega(\eta)) = S_{f,\mathrm{bu}}(\overline{\omega}) + \mathcal{O}(\xi_s)$. In this case, this term is seen as a constant with respect to integration along ω. The resonance component associated with the resonance peak in the positive range of frequencies therefore reads

$$\sigma_{q,\mathrm{R}}^2 = \frac{\overline{\omega}\,S_{f,\mathrm{bu}}(\overline{\omega})}{2\xi_s k_s^2}\int_{-\infty}^{+\infty}\frac{d\eta}{\alpha\eta^2 + \beta\eta + \gamma} = \frac{\overline{\omega}\,S_{f,\mathrm{bu}}(\overline{\omega})}{2\xi_s k_s^2}\left(\frac{2\pi}{\sqrt{4\alpha\gamma - \beta^2}}\right) \tag{42}$$

which constitutes the extension of the resonant component to high damping gradient structures. Accordingly, the superposition of the background and resonant components gives an estimate of the variance of the response

$$\sigma_q^2 = \sigma_{q,B}^2 + \frac{\overline{\omega}\,S_{f,\mathrm{bu}}(\overline{\omega})}{2\xi_{\mathrm{sk}_s}^2}\left(\frac{2\pi}{\sqrt{4\alpha\gamma - \beta^2}}\right) \tag{43}$$

To illustrate the gain in accuracy brought with this additional term, the results of the first (B)+(R1) and the second (B)+(R2) methods are compared for the Golden Gate application in Fig. 8, showing a perfect superimposition. It is seen in Fig. 3-c that the scaled damping gradient remains very low, indicating that the gain in accuracy is highly limited.

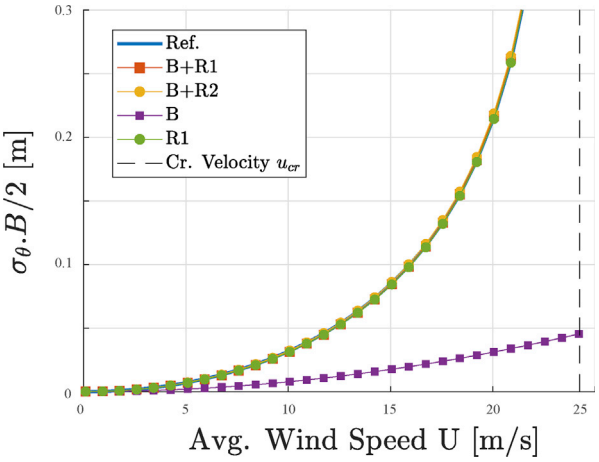

Fig. 8. Scaled standard deviations obtained from background component (B), resonant components (R), and the sum of them (B)+(R). (R1) assumes that the damping gradient is negligible, while (R2) drops this assumption.

References

Abbas, Tajammal, Kavrakov, Igor, Morgenthal, Guido, 2017. Methods for flutter stability analysis of long-span bridges: a review. In: Proceedings of the Institution of Civil Engineers-Bridge Engineering, vol. 170. Thomas Telford Ltd, pp. 271–310.

Amandolese, Xavier, Michelin, Sébastien, Choquel, M., 2013. Low speed flutter and limit cycle oscillations of a two-degree-of-freedom flat plate in a wind tunnel. J. Fluid Struct. 43, 244–255.

Andrianne, Thomas, de Ville de Goyet, Vincent, 2016. Mitigation of the torsional flutter phenomenon of bridge deck section during a lifting phase. In: 8th International Colloquium on Bluff Body Aerodynamics and Application.

Argentini, Tommaso, Pagani, A., Rocchi, Daniele, Alberto, Zasso, 2014. Monte Carlo analysis of total damping and flutter speed of a long span bridge: effects of structural and aerodynamic uncertainties. J. Wind Eng. Ind. Aerod. 128, 90–104.

Bisplinghoff, Raymond L., Ashley, Holt, 2013. Principles of Aeroelasticity. Courier Corporation.

Canor, Thomas, Caracoglia, Luca, Vincent, Denoël, 2015. Application of random eigenvalue analysis to assess bridge flutter probability. J. Wind Eng. Ind. Aerod. 140, 79–86.

Caracoglia, Luca, Jones, Nicholas P., 2003. Time domain vs. frequency domain characterisation of aeroelastic forces for bridge sections. J. Wind Eng. Ind. Aerod. 91 (3), 371–402.

Chen, Xinzhong, 2007. Improved understanding of bimodal coupled bridge flutter based on closed-form solutions. J. Struct. Eng. 133 (1), 22–31.

Chen, Xinzhong, Kareem, Ahsan, 2008. Identification of critical structural modes and flutter derivatives for predicting coupled bridge flutter. J. Wind Eng. Ind. Aerod. 96 (10–11), 1856–1870.

Chen, Xinzhong, Matsumoto, Masaru, Kareem, Ahsan, 2000. Aerodynamic coupling effects on flutter and buffeting of bridges. J. Eng. Mech. 126 (1), 17–26.

Cheng, Jin, Cai, C.S., Xiao, Ru-cheng, Chen, S.R., 2005. Flutter reliability analysis of suspension bridges. J. Wind Eng. Ind. Aerod. 93 (10), 757–775.

Davenport, Alan G., 1962. The response of slender, line-like structures to a gusty wind. Proc. Inst. Civ. Eng. 23 (3), 389–408.

Denoël, Vincent, 2009. Estimation of modal correlation coefficients from background and resonant responses. Struct. Eng. Mech.: Int. J. 32 (6), 725–740.

Denoël, Vincent, 2011. On the background and biresonant components of the random response of single degree-of-freedom systems under non-Gaussian random loading. Eng. Struct. 33 (8), 2271–2283.

Denoël, Vincent, 2015. Multiple timescale spectral analysis. Probabilist. Eng. Mech. 39, 69–86.

Denoël, Vincent, Degée, Hervé, 2009. Asymptotic expansion of slightly coupled modal dynamic transfer functions. J. Sound Vib. 328 (1–2), 1–8.

Diana, Giorgio, Stoyanoff, Stoyan, Aas-Jakobsen, Ketil, Allsop, Andrew, Andersen, Michael, Argentini, Tommaso, Montoya, Miguel Cid, Hernandez, Santiago, Jurado, Jose Angel, Katsuchi, Hiroshi, Kavrakov, Igor, Kim, Ho-Kyung, Larose, Guy, Larsen, Allan, Morgenthal, Guido, Oiseth, Ole, Omarini, Simone, Rocchi, Daniele, Svendsen, Martin, Wu, Teng, 2019. Iabse task group 3.1 benchmark results. part 1: numerical analysis of a two-degree-of-freedom bridge deck section based on analytical aerodynamics. Struct. Eng. Int. 1–10, 0(0).

Dimitriadis, Grigorios, 2017. Introduction to Nonlinear Aeroelasticity. John Wiley & Sons.

EN, 2009. EN 1991-1-4:2005+A1 Eurocode 1: Actions on Structures - Part 1-4. General actions - Wind actions, Brussels. CEN.

Foucriat, Cremona, 2002. *Comportement au vent des ponts*, chapter Notions d'aérodynamique et d'élasticité, page 3.30. Association Francaise de Génie Civil.

Hémon, Pascal, 2006. Vibrations des structures couplées avec le vent. Editions Ecole Polytechnique.

Hinch, E John, 1991. Perturbation Methods.

Jain, Anurag, Jones, Nicholas P., Scanlan, Robert H., 1996. Coupled flutter and buffeting analysis of long-span bridges. J. Struct. Eng. 122 (7), 716–725.

Jones, R.T., 1940. NACA Technical Report. The Unsteady Lift on a Wing of Finite Aspect Ratio, 681.

Kareem, Ahsan, Tamura, Yukio, 2013. Advanced Structural Wind Engineering. Springer.

Katsuchi, H., Jones, N.P., Scanlan, R.H., Akiyama, H., 1998. Multi-mode flutter and buffeting analysis of the akashi-kaikyo bridge. J. Wind Eng. Ind. Aerod. 77, 431–441.

Larsen, Allan, 1998. Advances in aeroelastic analyses of suspension and cable-stayed bridges. J. Wind Eng. Ind. Aerod. 74-76, 73–90.

Larsen, Allan, 2000. Aerodynamics of the tacoma narrows bridge - 60 years later. Struct. Eng. Int. 10 (4), 243–248.

Miyata, T., Yamada, H., 1990. Coupled flutter estimate of a suspension bridge. J. Wind Eng. Ind. Aerod. 33 (1–2), 341–348.

Pindado, S., Meseguer, J., Franchini, S., 2005. The influence of the section shape of box-girder decks on the steady aerodynamic yawing moment of double cantilever bridges under construction. J. Wind Eng. Ind. Aerod. 93 (7), 547–555.

Press, William H., Teukolsky, Saul A., Vetterling, William T., Flannery, Brian P., 2007. Numerical Recipes 3rd Edition: the Art of Scientific Computing. Cambridge university press.

Sarkar, Partha P., Jones, Nicholas P., Scanlan, Robert H., 1992. System identification for estimation of flutter derivatives. J. Wind Eng. Ind. Aerod. 42 (1–3), 1243–1254.

Sarkar, Partha P., Caracoglia, Luca, Haan Jr., Frederick L., Sato, Hiroshi, Murakoshi, Jun, 2009. Comparative and sensitivity study of flutter derivatives of selected bridge deck sections, part 1: analysis of inter-laboratory experimental data. Eng. Struct. 31 (1), 158–169.

Scanlan, Robert H., 1993. Problematics in formulation of wind-force models for bridge decks. J. Eng. Mech. 119 (7), 1353–1375.

Scanlan, Robert H., Jones, Nicholas P., 1990. Aeroelastic analysis of cable-stayed bridges. J. Struct. Eng. 116 (2), 279–297.

Scanlan, Robert H., Tomo, J., 1971. Air foil and bridge deck flutter derivatives. J. Soil Mech. Found Div. 97 (6), 1717–1737.

Simiu, Emil, Scanlan, Robert H., 1996. Wind Effects on Structures: Fundamentals and Applications to Design.

Theodorsen, Theodore, 1935. NACA Report. General Theory of Aerodynamic Instability and the mechanism of Flutter, 496.

Tubino, Federica, 2005. Relationships among aerodynamic admittance functions, flutter derivatives and static coefficients for long-span bridges. J. Wind Eng. Ind. Aerod. 93 (12), 929–950.

Zhang, C.G., 2007. Soft Flutter and Parameters Identification of Nonlinear Self-Excited Aerodynamic Force of Bridge Girder. Tongji University, China.